Molecular Dipole Function Inversion from Time Dependent Probability Density and Electric Field Data

Wusheng Zhu and Herschel Rabitz*

Department of Chemistry, Princeton University, Princeton, New Jersey 08544-1009

Received: June 2, 1999; In Final Form: August 3, 1999

A noniterative quantum mechanical algorithm is presented to extract the dipole function from time dependent probability density and external electric field data. The algorithm determines the dipole function as the solution of an exact linear integral equation without the need to solve the Schrödinger equation. The inversion in regular regions of the dipole is accurate and stable under perturbations from noisy data. The regular regions of the dipole are automatically identified by the algorithm, and Tikhonov regularization is employed. There is much freedom in the external electric field with the best choices generally producing broad excitations of many eigenstates. Field designs may be estimated from the Hamiltonian or through closed loop learning techniques in the laboratory. The inversion algorithm is tested in a simulation for O−H, which shows that the algorithm is very reliable. Since the inversion algorithm is fast, it is argued that closed loop laboratory learning techniques may be applied to optimally attain the dipole function in a desired region, whether local or as broad as possible, within the scope of the dynamics and control field capabilities.

1. Introduction

The dipole moment function is valuable for analyzing molecular spectra and as input into the controlled manipulation of molecular dynamics. Ab initio quantum chemistry calculations[1,2] and the inversion of time-independent spectral data[3−5] are two traditional means for obtaining a dipole function. Each of these approaches has its own strengths and limitations. In some systems, the dipole moment over the domain of interest may have a simple form (e.g., a low order polynomial). In such a special circumstance, inversion of the dipole function reduces to determining the expansion coefficients often by least squares fitting of the spectral intensities. In this paper, we develop a new inversion algorithm which is operative regardless of the form of the dipole moment function in a system with a known potential.

Due to recent progress in ultrafast laser technology, it is becoming possible to generate time-dependent experimental data with increasingly higher spatial and temporal resolution at the molecular scale.[6−8] It remains an open issue whether such data will eventually be advantageous for extracting dipole moment functions, but the technology is rapidly evolving. Some inverse algorithm development for treating such data has been developed including the introduction of special inverse tracking techniques.[9] Attaining high quality dipole functions from temporal quantum observations calls for additional laboratory and algorithmic advances. In this paper, a new time-dependent quantum inversion algorithm will be explored for this purpose.

The field of quantum state measurement, including quantum tomography, or holography[10−13] has been receiving increasing attention. Some efforts have even attempted to measure both the amplitude and phase of a time-dependent wavepacket. However, these observations either call for prior knowledge of the Hamiltonian, specific reference states, or the assumption of detailed available information about the system optical coupling coefficients.[12,13] If only measurement of the probability density is sought by discarding the quantum dynamical phase, then the situation is dramatically different. There are a number of emerging measurement methods for obtaining the probability density data, including laser pump−dump electron diffraction;[14] ultrafast X-ray diffraction;[15] photoexcitation followed by autoionization of a core state;[16] photoelectron spectra with ultrafast pump−probe[17] and Coulomb explosion imaging.[18] Besides the probability density data $\rho(x, t)$, in order to invert the dipole function, it is also necessary to measure the laser electric field $\epsilon(t)$ providing the excitation. Experimental techniques, such as electrooptic probing,[19] frequency-resolved optical gating measurement,[20−22] and autocorrelation measurement,[23,24] are available for measuring the electric field. Generating controlled broad band laser fields may be achieved by existing filtering and chirping techniques.[25,26]

Stimulated by the increasing efforts at generating probability density and laser electric field data, this paper will examine its potential utility for determining molecular dipole moment functions. Although the wave function phase is lost in the probability density, we will show that $\rho(x, t)$ and $\epsilon(t)$ have sufficient information to admit a direct inversion algorithm. The paper will show that no special prior field designs are necessary to implement the inversion. Furthermore it will also be argued that closed loop learning control techniques applied in the laboratory can be employed to steer about the density for determining the dipole function in some desired region. A recent work introduced an algorithm analogous to the one here for extracting potential surfaces from probability density data.[27] Below we assume that the potential is available to sufficient accuracy by this means or some other method; the potential is not employed for any design purpose here, but it appears along with the laboratory data in the equation to be solved for the dipole function. We hope that the evident capabilities of the dipole inversion algorithm will stimulate further experimental advances to make the necessary data available for application.

10.1021/jp991767k CCC: $18.00
Published on Web 09/25/1999

2. Direct Time-Dependent Inversion Algorithm

For simplicity of illustration, only a one dimensional form of the algorithm will be presented here; it is rather evident how to generalize the formulation to multidimensions. For a system governed by the time-dependent Schrödinger equation under the dipole approximation for the field interaction,

$$i\frac{\partial}{\partial t}\psi(x,t)=\left[-\frac{1}{2m}\frac{\partial^2}{\partial x^2}+V(x)-\mu(x)\,\epsilon(t)\right]\psi(x,t),\quad t\geq 0 \tag{1}$$

we have Ehrenfest's relation

$$\int_{-\infty}^{\infty}\epsilon(t)\,\rho(x,t)\frac{\partial\mu(x)}{\partial x}\,\mathrm{d}x=m\frac{d^2}{dt^2}\int_{-\infty}^{\infty}x\rho(x,t)\,\mathrm{d}x+\int_{-\infty}^{\infty}\rho(x,t)\frac{\partial V(x)}{\partial x}\,\mathrm{d}x,\quad t\geq 0 \tag{2}$$

where $\rho(x,t)$ vanishes toward the boundary $|x|\rightarrow\infty$ at any finite time. Given the probability density data $\rho(x,t)$ and the field data $\epsilon(t)$, then eq 2 provides an exact integral equation to solve for the dipole gradient $\partial\mu(x)/\partial x$. There is no need to solve the Schrödinger equation as part of the inversion algorithm. The time $t=0$ is defined as the point for initiation of observations of the external field $\epsilon(t)$ and probability density $\rho(x,t)$ data. The field actually may be started at a time $t<0$, while the observation process can be started at any convenient time defined as $t=0$ just so the data over the interval $0\leq t\leq T$ captures sufficient information for inversion. The dipole can be extracted from its gradient inverted from eq 2:

$$\mu(y)=\mu(y')+\int_{y'}^{y}\frac{\partial\mu(x)}{\partial x}\,\mathrm{d}x \tag{3}$$

where y' is a point where $\mu(y')$ is known. One example is $y'\rightarrow\infty$ for atoms dissociating as neutrals, where the dipole vanishes, $\mu(\infty)=0$. In practice it is usually sufficient to determine the dipole up to an arbitrary constant. The integration operation in eq 3 tends to further reduce residual noise left in the dipole gradient from inversion.

As discussed below, there is much flexibility in the form of the excited wavepacket driven by $\epsilon(t)$, although its structure effects the inversion process. Closed loop laboratory learning techniques may be employed to aid this process if desired, as explained in section 6.

If the excited wavepacket $\psi(x,t)$ in eq 2 is a superposition of a finite number of discrete bound eigenstates,

$$\psi(x,t)=\sum_{n=1}^{N}a_n\phi_n(x)\,\mathrm{e}^{-iE_nt} \tag{4}$$

then inversion to extract the dipole by eq 2, or by any means, will be an ill-posed problem because $\psi(x,t)$ only has significant support in a finite region of the spatial domain (i.e., $\mu(x)$ cannot be determined well everywhere). If $\psi(x,t)$ also includes an arbitrary number of continuum eigenstates,

$$\psi(x,t)=\sum_{n=1}^{N}a_n\phi_n(x)\,\mathrm{e}^{-iE_nt}+\int_0^{\infty}b(E)\phi_E(x)\,\mathrm{e}^{-iEt}\mathrm{d}E \tag{5}$$

then in principle the kernel $\rho(x,t)$ on the LHS of eq 2 might have full rank arresting the problem of ill-posedness if the amplitude $b(E)$ covers a sufficiently large energy band. In practice, a typical situation will involve the superposition of a finite number of eigenstates as shown in eq 4, and the analysis here aims to demonstrate what can be determined regarding the dipole under these conditions. Because of the inherent ill-posedness of the inversion problem, generally we can only achieve a globally approximate inverse solution. Under these conditions, it is suggestive to put together all of the data to find the best inverse solution through minimization of $\mathbf{J}_0$:

$$\mathbf{J}_0=\frac{1}{T}\int_0^T\left(\int_{-\infty}^{\infty}\epsilon(t)\,\rho(x,t)\frac{\partial\mu(x)}{\partial x}\,\mathrm{d}x-\int_{-\infty}^{\infty}\rho(x,t)\frac{\partial V(x)}{\partial x}\,\mathrm{d}x-m\frac{d^2}{dt^2}\int_{-\infty}^{\infty}x\rho(x,t)\,\mathrm{d}x\right)^2\mathrm{d}t \tag{6}$$

where it would be desirable for T to be as large as possible in keeping with experimental capabilities. Minimizing $\mathbf{J}_0$ with respect to the dipole gradient will lead to the following equation:

$$\int_{-\infty}^{\infty}\left(\frac{1}{T}\int_0^T[\epsilon(t)]^2\,\rho(x',t)\rho(x,t)\,\mathrm{d}t\right)\frac{\partial\mu(x)}{\partial x}\,\mathrm{d}x=\frac{1}{T}\int_0^T\epsilon(t)\rho(x',t)\left(m\frac{d^2}{dt^2}\int_{-\infty}^{\infty}x\rho(x,t)\,\mathrm{d}x+\int_{-\infty}^{\infty}\rho(x,t)\frac{\partial V(t)}{\partial x}\,\mathrm{d}x\right)\mathrm{d}t \tag{7}$$

The kernel $A(x',x)$ for this integral equation

$$A(x',x)=\frac{1}{T}\int_0^T[\epsilon(t)]^2\,\rho(x',t)\rho(x,t)\,\mathrm{d}t \tag{8}$$

is positive semidefinite. Equation 7 still may leave a singular or ill-posed problem, as $A(x',x)$ generally has a null space. The rank of $A(x',x)$ can be qualitatively understood from considering the wave function in eq 4 as a superposition of N discrete eigenstates $\phi_n(x)$, $n=1,2,\ldots,N$. Often $\phi_n(x)$ is a polynomial, with the highest order being x^n, modulated by a shape factor which will not change the number of roots of $\phi_n(x)$. In such polynomial cases, the eigenvalue λ_i and eigenfunction $\zeta_i(x)$ for the kernel $A(x',x)$ will satisfy

$$\int_{-\infty}^{\infty}A(x',x)\zeta_i(x)\mathrm{d}x=\lambda_i\zeta_i(x') \tag{9}$$

which can be explicitly written as

$$\frac{1}{T}\int_0^T\{[\epsilon(t)]^2\sum_{n=1}^{N}a_n^*\,\phi_n^*(x')\,\mathrm{e}^{iE_nt}\sum_{m=1}^{N}a_m\phi_m(x')\,\mathrm{e}^{-iE_mt}\int_{-\infty}^{\infty}\sum_{k=1}^{N}a_k^*\,\phi_k^*(x)\,\mathrm{e}^{iE_kt}\sum_{l=1}^{N}a_l\phi_l(x)\,\mathrm{e}^{-iE_lt}\,\zeta_i(x)\,\mathrm{d}x\}\,\mathrm{d}t=\lambda_i\zeta_i(x') \tag{10}$$

On the left-hand side of eq 10, the variables x and t are integrated over so that only variable x' survives. And it is evident that $(x')^{2N}$ is the highest order term on the LHS. Thus $\zeta_i(x')$ on the RHS must be a polynomial, perhaps modulated by a shape factor, of up to order $2N$, and then the rank of $A(x',x)$ will at most be $2N$. The null space of $A(x',x)$ causes the singularity of the inverse problem. Furthermore, noise in the measured probability density data can mask small differences among some features of $A(x',x)$ to raise artificial data correlations which may exacerbate the ill-posedness problem. Under these conditions, regularization will generally be necessary, as introduced below.

3. Regularization

Since equation 7 is generally ill-posed, at least because of the probability density being small in some regions, then the

corresponding dipole will be ill-defined in those locations. Therefore, a feasible inversion algorithm should be able to (a) identify the ill-defined regions and (b) employ an appropriate form of regularization[28] to eliminate the singular behavior.

Possible means of regularization include truncated singular value decomposition (TSVD)[29] and Tikhonov schemes.[30] We adopt the latter form since it is necessary to add only an extra term to the original functional $\mathbf{J}_0$ to form a new functional $\mathbf{J}_1$

$$\mathbf{J}_1 = \frac{1}{T}\int_0^T \left(\int_{-\infty}^{\infty} \epsilon(t)\, \rho(x, t)\, \frac{\partial \mu(x)}{\partial x}\, \mathrm{d}x - \int_{-\infty}^{\infty} \rho(x, t)\, \frac{\partial V(x)}{\partial x}\, \mathrm{d}x - m\frac{d^2}{dt^2}\int_{-\infty}^{\infty} x\rho(x, t)\, \mathrm{d}x \right)^2 \mathrm{d}t + \alpha \int_{-\infty}^{\infty} \left(\frac{\partial \mu(x)}{\partial x} \right)^2 \mathrm{d}x \quad (11)$$

where the regularization parameter α is a suitably small positive number. The regularization term acts to remove the singular behavior of the solution, especially oscillatory features, by extracting a solution with both good accuracy as well as proper smoothness. Minimizing $\mathbf{J}_1$ with respect to the dipole gradient will lead to the following equation for the regularized solution:

$$\int_{-\infty}^{\infty} \left[\frac{1}{T}\int_0^T [\epsilon(t)]^2\, \rho(x', t)\, \rho(x, t)\, \mathrm{d}t + \delta(x' - x)\, \alpha \right] \frac{\partial \mu(x)}{\partial x}\, \mathrm{d}x = \frac{1}{T}\int_0^T \epsilon(t)\, \rho(x', t) \left(m\frac{d^2}{dt^2}\int_{-\infty}^{\infty} x\rho(x, t)\, \mathrm{d}x + \int_{-\infty}^{\infty} \rho(x, t)\, \frac{\partial V(x)}{\partial x}\, \mathrm{d}x \right) \mathrm{d}t \quad (12)$$

which can be rewritten as

$$\int_{-\infty}^{\infty} [A(x', x) + \delta(x' - x)\, \alpha]\, \frac{\partial \mu(x)}{\partial x}\, \mathrm{d}x = b(x') \quad (13)$$

where $A(x', x)$ is given in equation 8 and $b(x')$ is defined as the right-hand side of eq 12. In practice, eq 13 will be solved on a discrete grid, and a matrix-vector form becomes

$$(\mathbf{A} + \alpha\mathbf{I})\, \mathbf{u}_x = \mathbf{b} \quad (14)$$

where $\mathbf{I}$ is a unit matrix and $\mathbf{u}_x$ and $\mathbf{b}$ are column vectors. The matrix $\mathbf{A}$ is positive semi-definite with eigenvalues $\lambda_i \geq 0$, and the inverse of the matrix is well behaved with $(\lambda_i + \alpha) > 0$ making the inversion unique and singularity free. Since α is a small number, it has little impact on the significantly nonzero eigenvalues of $\mathbf{A}$, which is essential for the regularized solution to be a good approximation to the true dipole function in the well-defined regular region.

4. Stability Analysis for Noisy Data

Because $\mathbf{A}$ and $\mathbf{b}$ are generated from the observed $\rho(x, t)$ and $\epsilon(t)$ data, they will be subject to measurement and/or numerical errors. In addition, $\mathbf{b}$ depends on the potential which will also be subject to some error. It is important to address the effect that perturbations in $\mathbf{A}$ and $\mathbf{b}$ have on the solution $\mathbf{u}_x$. Errors enter from the deviation in measurements of $\rho(x, t)$ and $\epsilon(t)$, imprecision of the potential surface obtained elsewhere, and the time derivative of the expectation value of x in $\mathbf{b}$ [cf. the right-hand side of eq 12]; however, both $\mathbf{A}$ and $\mathbf{b}$ involve time integration which will reduce the error level to some degree. If any residual errors change $\mathbf{A}$ to $\mathbf{A} + \delta\mathbf{A}$, and $\mathbf{b}$ to $\mathbf{b} + \delta\mathbf{b}$, then these disturbances will introduce corresponding changes in $\mathbf{u}_x$ to $\mathbf{u}_x + \delta\mathbf{u}_x$. The perturbed equation is given by

$$(\mathbf{A} + \delta\mathbf{A} + \alpha\mathbf{I})\, (\mathbf{u}_x + \delta\mathbf{u}_x) = \mathbf{b} + \delta\mathbf{b} \quad (15)$$

Subtracting eq 14 from eq 15 yields

$$\delta\mathbf{u}_x = (\mathbf{A} + \delta\mathbf{A} + \alpha\mathbf{I})^{-1}\, (\delta\mathbf{b} - \delta\mathbf{A}\cdot\mathbf{u}_x) \quad (16)$$

Here we desire to put a bound on $\delta\mathbf{u}_x$ in relation to the norm of $\delta\mathbf{b}$ and $\delta\mathbf{A}$. Denoting $||\cdot||$ as a suitable norm (e.g., $||\cdot||_F$, $||\cdot||_1$, $||\cdot||_2$, or $||\cdot||_\infty$) of the corresponding matrix or vector, then from eq 16 we have

$$\begin{aligned} ||\delta\mathbf{u}_x|| &= ||(\mathbf{A} + \delta\mathbf{A} + \alpha\mathbf{I})^{-1}\, (\delta\mathbf{b} - \delta\mathbf{A}\, \mathbf{u}_x)|| \\ &\leq ||(\mathbf{A} + \delta\mathbf{A} + \alpha\mathbf{I})^{-1}||\, ||\delta\mathbf{b} - \delta\mathbf{A}\, \mathbf{u}_x|| \\ &\leq ||(\mathbf{A} + \alpha\mathbf{I})^{-1}||\, ||[\mathbf{I} + (\mathbf{A} + \alpha\mathbf{I})^{-1}\, \delta\mathbf{A}]^{-1}||\, (||\delta\mathbf{b}|| + ||\delta\mathbf{A}||\, ||\mathbf{u}_x||) \end{aligned} \quad (17)$$

Therefore, since $||\mathbf{b}|| \leq ||\mathbf{A} + \alpha\mathbf{I}||\, ||\mathbf{u}_x||$ from eq 14, then eq 17 yields

$$\frac{||\delta\mathbf{u}_x||}{||\mathbf{u}_x||} \leq ||\mathbf{A} + \alpha\mathbf{I}||\, ||(\mathbf{A} + \alpha\mathbf{I})^{-1}||\, ||[\mathbf{I} + (\mathbf{A} + \alpha\mathbf{I})^{-1}\, \delta\mathbf{A}]^{-1}|| \left(\frac{||\delta\mathbf{b}||}{||\mathbf{b}||} + \frac{||\delta\mathbf{A}||}{||\mathbf{A} + \alpha\mathbf{I}||} \right) \quad (18)$$

Conventionally, the data noise level is assumed small to satisfy $||(\mathbf{A} + \alpha\mathbf{I})^{-1}\, \delta\mathbf{A}|| < 1$, and the condition number of matrix $\mathbf{M}$ is defined as $c(\mathbf{M}) \equiv ||\mathbf{M}||\, ||\mathbf{M}^{-1}||$, which can further simplify eq 18 to be

$$\frac{||\delta\mathbf{u}_x||}{||\mathbf{u}_x||} \leq \frac{c(\mathbf{A} + \alpha\mathbf{I})}{1 - ||(\mathbf{A} + \alpha\mathbf{I})^{-1}\delta\mathbf{A})||} \left(\frac{||\delta\mathbf{b}||}{||\mathbf{b}||} + \frac{||\delta\mathbf{A}||}{||\mathbf{A} + \alpha\mathbf{I}||} \right) \quad (19)$$

From eq 19, we see that after regularization the relative error in the solution is bounded by the relative errors in the data. If $\alpha = 0$ (i.e., no regularization), the condition number of the singular matrix $\mathbf{A}$ will be very large leading to significant deviation in the solution. Thus the regularization serves to stabilize the inverse solution with respect to noisy data. This point will be explored in the simulated inversion below by comparing the regularized and unregularized solutions.

A more elaborate analysis may also be carried out showing the detailed relationship between small disturbances in $\delta\rho(x, t)$ and $\delta\epsilon(t)$ and resultant error in $\mathbf{u}_x$. It is expected that small perturbations in the probability density and the external field will result in small perturbations in $\mathbf{u}_x$, as an analog to the results of an error analysis of a similar inversion algorithm for the potential function.[27]

5. Simulated Inversion

In the simulated inversion, we choose O−H as an illustration; all the parameters are expressed in atomic units (au). To execute the inversion, the potential is assumed to be known. For purposes of simulation here we take the following Morse potential[31] as an adequate description of the O−H electronic ground state

$$V(x) = D_0[\mathrm{e}^{-\beta(x-x_0)} - 1]^2 - D_0 \quad (20)$$

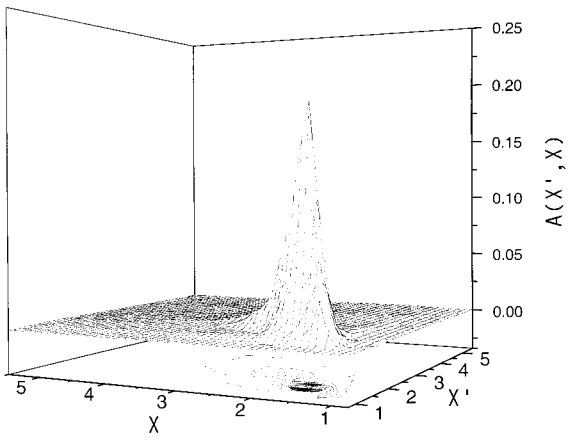

Figure 1. Three-dimensional and contour plots showing the coordinate dependence of the kernel $A(x', x)$ in the first simulated inversion. The significantly nonzero region roughly defines the regular domain for inversion, while the nearly zero region is singular for inversion.

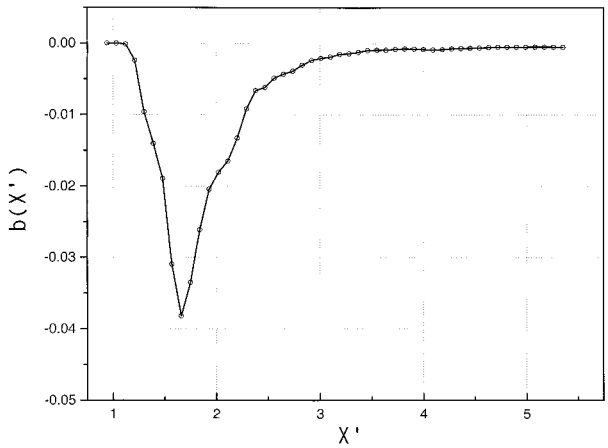

Figure 2. The coordinate dependence of the inhomogeneity $b(x')$. The asymptotic regions of $x' < 1.1$ and $x' > 3.5$ show similar behavior to the singular domains of $A(x', x)$ shown in Figure 1.

where $D_0 = 0.1994$, $\beta = 1.189$, and $x_0 = 1.821$. The dipole moment as a function of the O−H bond length is taken as[32]

$$\mu(x) = \mu_0 x \, e^{-x/x^*} \tag{21}$$

where $\mu_0 = 3.088$ and $x^* = 0.6$. In the simulation, we will adopt the dipole function in eq 21 to generate "experimental" probability density data and apply the inversion algorithm in eq 12 to extract the dipole to test the behavior of the algorithm.

The molecule is assumed to be in the vibrational ground state when the laser field is turned on. It is evident that generally the best excitation pulses in terms of maximum information content will be those that result in the wave packet having the largest number of eigenstates. In the following treatment, the implementation of the algorithm will be displayed with two different laser fields. The examples will show that the regular regions of the dipole depend on the nature of the excitation laser field and the resultant wave packet. In the first simulation example, a broad band laser field is rather arbitrarily chosen as

$$\epsilon(t) = 0.35 \cos(t^2/160000) \exp[-\sin(t^2/10000)] \tag{22}$$

As evident from the simulations, there is no strong sensitivity to subtle details in the field. For example, the field may just as well be turned on/off slowly in keeping with laser capabilities. In the first step of the inversion, the experimental probability density and the external field data are used to construct the kernel in eq 8. The corresponding kernel $A(x', x)$ is plotted in Figure 1. Figure 1 roughly identifies the regular region, and the corresponding singular region (i.e., where the matrix $A(x', x)$ is zero, constant, or contains correlations in two rows or columns) for inversion. In Figure 2, $b(x')$ is plotted to display the invertible region in another way. The elements of vector **b** become almost zero in the regions of $x' < 1.1$ and $x' > 3.5$, which is consistent with the null space of $A(x', x)$.

In the second step, the number of points that can be inverted on the dipole is estimated from the number of nonzero eigenvalues of the kernel matrix. As analyzed in section 2, the number of significant nonzero eigenvalues of the kernel matrix $A(x', x)$ in eq 8 dictates the maximum amount of invertible information (e.g., discrete points) of the dipole that may be determined. In the simulation, there are about 50 nonzero eigenvalues (some contributions come from continuum eigenstates) within the condition number of 10^{14}. This indicates that roughly the same number of discrete points of the dipole may be determined; a few points more or less will not cause any trouble due to the use of regularization. We choose the discrete number of points to be 50, uniformly spaced over the inversion range $x \in [0.94, 5.35]$, and $T = 2.0 \times 10^3$ is taken to carry out the time integration in the kernel. The points are shown in Figure 2.

In the third step, the Tikhonov regularization procedure is applied to invert the matrix kernel to obtain the dipole gradient. In order to set flags to distinguish the regular and singular regions, we utilize the property that the solution in the singular regions is relatively sensitive, while in the regular region it is relatively stable with respect to changes of the regularization parameter (as well as the data noise level). Two extreme cases are compared. One is $\alpha = 0$ corresponding to no regularization, while the other is $\alpha = \alpha_{opt}$ corresponding to optimal regularization. α_{opt} is determined by scanning over α to find the global minimum point of the functional $\mathbf{J}_2$

$$\mathbf{J}_2 = \frac{1}{T}\int_0^T \left(\int_{-\infty}^{\infty} \epsilon(t)\, \rho(x, t) \frac{\partial \mu(x, \alpha)}{\partial x} \, dx - \int_{-\infty}^{\infty} \rho(x, t) \frac{\partial V(x)}{\partial x} \, dx - m \frac{d^2}{dt^2} \int_{-\infty}^{\infty} x \rho(x, t) \, dx \right)^2 dt \tag{23}$$

which minimizes the residual of a solution similar to that for $\mathbf{J}_0$ in eq 6, except that now the solution is α-dependent. For each α_i, the gradient $\partial\mu(x, \alpha_i)/\partial x$ in eq 23 is the solution that minimizes $\mathbf{J}_1$ at $\alpha = \alpha_i$. The regular region for inversion was defined as the domain where the solution difference between $\alpha = \alpha_{opt}$ and $\alpha = 0$ changed by no more than a tolerance of 1% (the value reflects, although it is not necessarily the same as, the level of numerical and measurement errors); the counterpart domain is denoted as the singular region. Figure 3 plots the relative error of the solution change between $\alpha = \alpha_{opt}$ and $\alpha = 0$. Under the 1% criterion, the regular region is continuous $x \in [1.30, 3.55]$ and shown by grey shadow, while the singular regions are $x \in (0, 1.30)$ and $x \in (3.55, \infty)$ (the regular and singular regions could have complex disjoint structure for the inversion of multidimensional systems). The inverted dipole gradient for the two cases is displayed in Figure 4. As expected, the optimal regularized solution preserves good accuracy in the regular region, and it achieves global smoothness in both the regular and singular regions. In this example, the field happens to be especially attractive, as the inversion even without regularization is quite good.

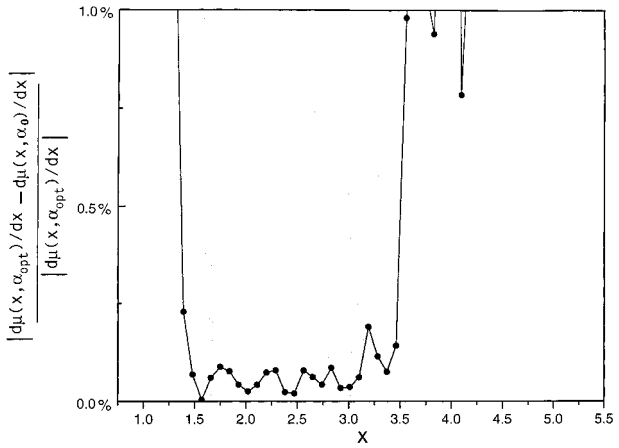

Figure 3. Relative change of the inverted dipole derivative when the regularization parameter changes from the optimal value $\alpha = \alpha_{opt}$ to $\alpha = 0$ (indicated as α_0 in the plot). The grey shadow region $x \in [1.30, 3.55]$ defines where the solution change is less than 1%, which is referred to as the regular region.

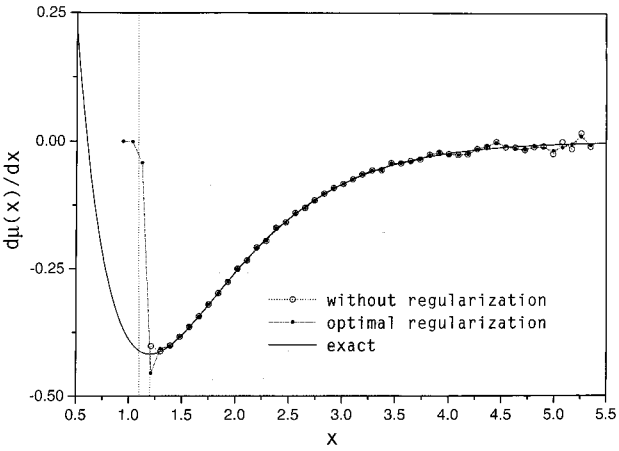

Figure 4. Comparison between the exact and the two inverted dipole gradients, corresponding to optimal regularization and no regularization. In the grey shadow regular region, both inversions are quite accurate. In the singular regions, the inversions are uncertain.

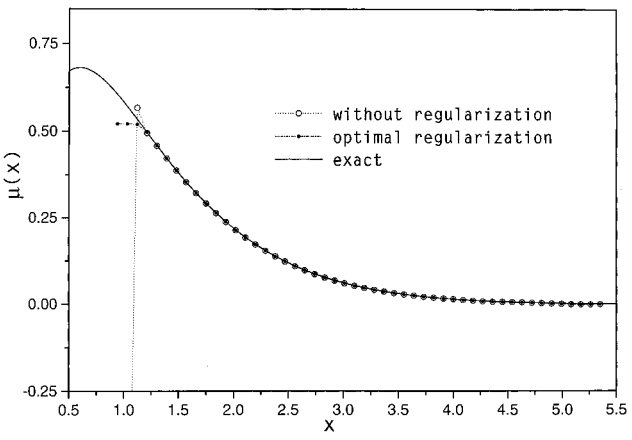

Figure 5. Comparison between the exact and the two extracted dipoles from inversion with optimal regularization and without regularization. In the singular regions, the dipoles are uncertain. In the regular region, the both extracted dipoles are very accurate. Knowledge of an absolute reference point in the regular region is necessary to eliminate a possibly dynamically irrelevant constant shift.

In the fourth step, eq 3 is adopted to extract the dipole from the inverted dipole gradient. Figure 5 compares the dipoles extracted from the dipole gradients by inversion with $\alpha = 0$ and $\alpha = \alpha_{opt}$. For this excitation field, both dipoles are in excellent agreement with the truth in the regular region. In general, the inverted dipole in the regular region will differ from the truth by a constant which is dynamically irrelevant from the integration in eq 3.

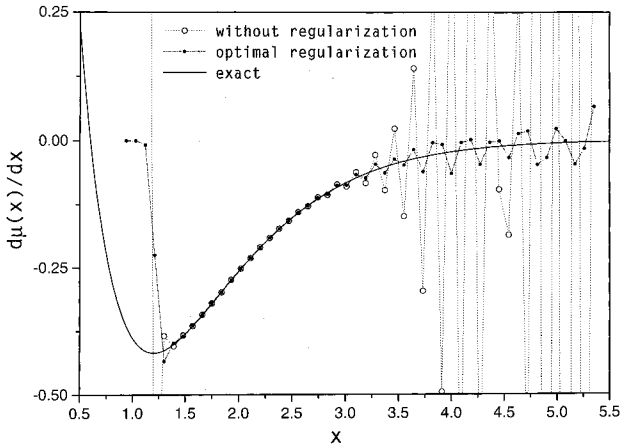

Figure 6. Comparison between the exact and the two inverted dipole gradients, corresponding to optimal regularization and no regularization. The inversion with optimal regularization is smoother than that without regularization in the singular regions. In the grey shadow regular region, both inversions are quite accurate. In the singular regions, the inversions are uncertain. The same 1% criterion employed in Figure 3 is used to distinguish the regular and singular regions.

In the second simulated inversion, the laser field is chosen as

$$\epsilon(t) = 0.35 \cos(t^2/20000) \exp[-\sin(t^2/1000)] \quad (24)$$

which contains high frequency components inducing bound-continuum transitions but a reduced amount of frequency components inducing bound-bound transitions. Thus, the excitation for inversion purposes is not as appropriate as in the first example. In this case, the discrete number of points is still chosen to be 50, uniformly spaced over the inversion range $x \in [0.94, 5.35]$, and $T = 3.0 \times 10^3$ is taken as the time observation interval. Following the same inversion procedure as in the first example, we obtain the dipole gradients plotted in Figure 6 with optimal regularization and without regularization. The regular region for inversion is indicated by the grey shadow where $x \in [1.40, 2.90]$, and the other regions are singular for inversion. The range of the regular inverse region is narrower than that of the first example since the excited wavepacket contains less information about the dipole. Figure 7 shows the extracted dipoles. With no regularization, the inverted dipole in the regular region is very close to the true dipole except for a dynamically irrelevant constant shift, which arises from the residual of integration over the oscillatory singular region. With optimal regularization, the inverted dipole is in excellent agreement with the true function. In general, a finite constant shift will likely occur regardless of any regularization, unless independent information (e.g., a known dipole at a point in the regular region) is available which then can determine the reference dipole $\mu(y')$ in eq 3 at point y'.

6. Closed Loop Laboratory Learning Procedure

The analysis in the previous sections shows that a fast and reliable algorithm may be established to extract dipole functions from measurements of the electric field and ultrafast high resolution probability density data. The two illustrations in section 5 indicate a considerable degree of flexibility and

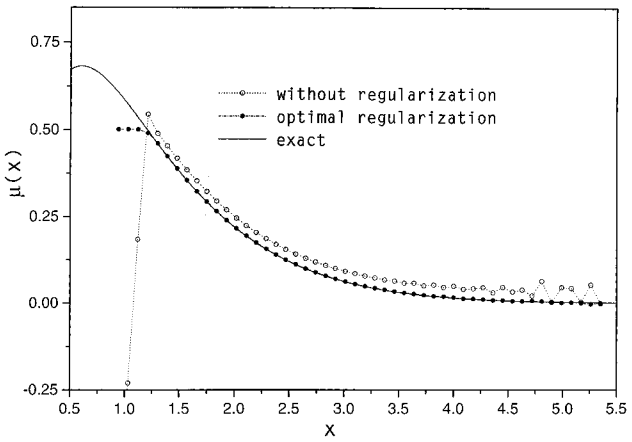

Figure 7. Comparison between the exact and the two extracted dipoles from inversion with optimal regularization and without regularization. In the singular regions, the dipoles are uncertain. In the regular region, the extracted dipole without regularization primarily differs from the truth by a constant, while that with optimal regularization is quite accurate with a small dynamically irrelevant constant.

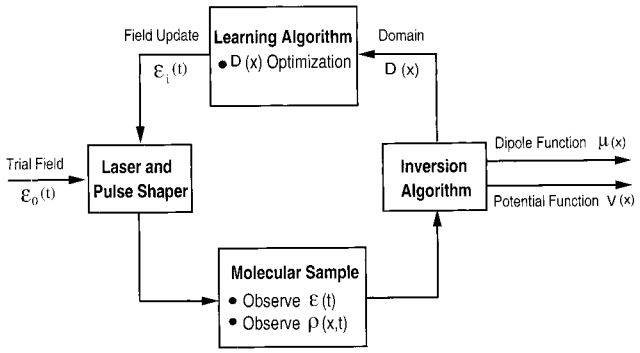

Figure 8. A closed loop laboratory learning process for extracting the dipole function $\mu(x)$ from high resolution probability density data $\rho(x, t)$ and observation of the electric field $\epsilon(t)$. The loop could be initiated by a trial field $\epsilon_0(t)$ from a design estimate. Each loop of the inversion algorithm would provide an update for $\mu(x)$, as well as an identification of the stable inversion domain $D(x)$ for optimization by the learning algorithm. This same logic may also be extended to extract the potential function $V(x)$ just from data $\rho(x, t)$.

robustness in the choice of the driving electric field. In any particular molecular application, there may be the additional desire to obtain the dipole either near some particular point, or perhaps, over the largest region possible. Although there will surely be no unique field meeting such additional criteria, merely guessing at the field would likely not be adequate. In addition, it is not possible to perform high accuracy prior field designs $\epsilon_0(t)$ since that would require knowledge of the dipole beforehand. Secondly, these efforts, even with the approximate dipole, call for solving the Schrödinger equation, which is an arduous task in multidimensions.

The above circumstances naturally lead to consideration of direct laboratory closed loop learning of the optimal laser field for the purpose of dipole function extraction from the data. This procedure has certain parallels, as well as important distinctions, with the earlier suggestion[33−37] of performing experiments to learn how to control molecules and steer them to some desired final product state. Such experiments have now been demonstrated[38−41] in the laboratory, and here, we propose their extension for inversion purposes.

Figure 8 shows a schematic diagram of the overall process where algorithms for inversion and learning are involved. Two features distinguish this process from the procedure of quantum learning control by a closed loop.[33−41] First, in the case of dipole extraction from the data, it is necessary to measure the electric field $\epsilon(t)$ rather than merely the stand-in laser "knob settings". Second, the actual inversion algorithm needs to be directly involved in the closed loop, as indicated. The output of the inversion algorithm ultimately is the desired dipole function, but during intermediate cycles of the loop, the inversion algorithm also provides specific characteristics $D(x)$ of the inversion process for employment in the learning algorithm, to suggest the next experiment for further refinement of the dipole function, etc. Considering the comments above, one case could be defined as $D(x) > 0$ prescribing the stable domain of the dipole inversion algorithm, and the learning algorithm would then be charged with the goal of maximizing the domain with respect to the control field, $\max_\epsilon D(x)$. Another circumstance concerns the desire to learn about the dipole in some prespecified locale $R(x) > 0$, such that the learning algorithm would then aim to minimize a suitable norm $\min_\epsilon \|D(x) - R(x)\|$. Any of a variety of learning algorithms should be effective for these purposes, based on prior theoretical studies[33−37] and currently emerging experience in the laboratory.[38−41]

Special attention to certain details is necessary for successful execution of this overall laboratory procedure for dipole determination. The two algorithmic operations and the data observations need to be sufficiently fast, such that the closed loop can be traversed in a reasonable period. It is anticipated that the number of iterations called for will be less than needed to meet typical closed-loop target state control objectives,[33−41] because the inversion problem shows evidence for broad latitude in the nature of the controls that could be successful. Nevertheless, the loop may be traversed hundreds of times or more. Fast field determination techniques are becoming available, which should aid this process. In addition, the strictly linear nature of the inversion algorithm should be an important factor, and the learning algorithms have already been demonstrated to be fast.[33−41] Incremental dipole upgrades could be introduced at each cycle, to further accelerate the inversion algorithm. We leave the suggestion of performing the experiments, as indicated in this section, for a full testing of the concept.

7. Summary

This paper presented a noniterative direct inversion algorithm to assess the feasibility of extracting the dipole moment function from emerging ultrafast high resolution probability density data and laser field measurements. Tikhonov regularization is introduced to cope with the singular nature of the problem, and an error analysis shows that the inversion is stable with respect to noisy data. A criterion was defined to distinguish the regular and singular regions from the experimental data. The algorithm was successfully tested for the inversion of a one-dimensional model system.

The inversion algorithm has several attractive features. The laser field can be chosen with much freedom. A desirable excitation is one which is sufficiently broad band to access many molecular eigenstates. The algorithm does not require solving the Schrödinger equation and it is noniterative through rigorous formulation as a linear integral equation. The fast speed and stability of the algorithm permit its direct use in the laboratory with a closed loop learning algorithm. In this fashion a full automation of the inversion process should be possible. In addition the general structure of the algorithm has a simple extension to multidimensions assuming such laboratory data becomes available. Regardless of dimension the algorithm still has the structure of a linear integral equation. However, a high

dimensional kernel would likely call for introducing special numerical methods, including iteration, for solution. In addition the data could be generated in a sequence of experiments where each experiment only drove the density to explore a moderate domain of configuration space. In this fashion each sequential inversion of the incremental data would not be computationally expensive regardless of the system dimension. A full examination of this matter is left to future studies.

Although this paper focused on dipole inversion from ultrafast high resolution observations, the logic involved may be married with that of a previous effort,[27] considering analogous techniques to extract the potential energy $V(x)$. In this case, only the probability density data is necessary, without observation of the field. The structure of this algorithm is essentially the same as for the dipole, producing the following regularized equations to be solved.

$$\int_{-\infty}^{\infty} [A'(x', x) + \delta(x' - x)\alpha'] \frac{\partial V(x)}{\partial x} dx = b'(x') \quad (25)$$

where $A'(x', x)$, and $b'(x')$ have the similar structure to their counterpart functions in eq 13. In this regard, Figure 8 includes the extension to consider the extraction of the potential and/or dipole function. This paper and previous theoretical[33−37] and experimental efforts[38−41] indicate that all the closed loop components are generally in hand for this effort. The crucial necessary new element is the probability density data, which we hope this paper helps stimulate.

Acknowledgment. One of the authors (HR) would like to express deep appreciation for many enjoyable interactions with Kent Wilson going back some 30 years. His central role in the quantum control and ultrafast dynamics community has been an inspiration for the field. The authors acknowledge support from the National Science Foundation and the Department of Defense.

References and Notes

(1) Partridge, H.; Schwenke, D. *J. Chem. Phys.* **1997**, *106*, 4618.
(2) Piecuch, P.; Spirko, V.; Paldus, J. *Mol. Phys.* **1998**, *94*, 55.
(3) Rawlins, W.; Person, J.; Fraser, M.; Miller, S.; Blumberg, W. *J. Chem. Phys*. **1998**, *109*, 3409.
(4) Ito, F.; Klose, P.; Nakanaga, T.; Takeo, H.; Jones, H. *J. Mol. Spectrosc.* **1999**, *194*, 17.
(5) Booth, J.; Hancock, G.; Toogood, M.; Mckendrick, K. *J. Phys. Chem*. **1996**, *100*, 47.
(6) Zewail, A. *J. Phys. Chem*. **1993**, *97*, 12427.
(7) Geiser, J.; Weber, P. *J. Chem. Phys*. **1998**, *108*, 8004.
(8) Rose-Petruck, C.; Jimenez, R.; Guo, T.; Cavalleri, A.; Siders, C.; Raksi, F.; Squier, J.; Walker, B.; Wilson, K.; Barty, C. *Nature* **1999**, *398*, 310.
(9) Lu, Z.; Rabitz, H. *Phys. Rev. A.* **1995**, *52*, 1961.
(10) Dunn, T.; Walmsley, I.; Mukamel, S. *Phys. Rev. Lett.* **1995**, *74*, 884.
(11) Walmsley, I.; Waxer, L. *J. Phys. B: At. Mol. Opt. Phys*. **1998**, *31*, 1825.
(12) Leichtle, C.; Schleich, W.; Averbukh, I.; Shapiro, M. *Phys. Rev. Lett*. **1998**, *80*, 1418.
(13) Weinacht, T.; Ahn, J.; Bucksbaum, P. *Phys. Rev. Lett.* **1998**, *80*, 5508.
(14) Williamson, J.; Cao, J.; Ihee, H.; Frey, H.; Zewail, A. *Nature* **1997**, *386*, 159.
(15) Krause, J.; Schafer, K.; Ben-Nun, M.; Wilson, K. *Phys. Rev. Lett*. **1997**, *79*, 4978.
(16) Jones, R. *Phys. Rev. A.* **1998**, *57*, 446.
(17) Assion, A.; Geisler, M.; Helbing, J.; Seyfried, V.; Baumert, T. *Phys. Rev. A.* **1996**, *54*, R4605.
(18) Stapelfeldt, H.; Constant, E.; Sakai, H.; Corkum, P. *Phys. Rev. A.* **1998**, *58*, 426.
(19) Wang, S.; Zhu, Z. *Appl. Phys. A.* **1995**, *60*, 425.
(20) Delong, K.; Fittinghoff, D.; Trebino, R.; Kohler, B.; Wilson, K. *Opt. Lett.* **1994**, *19*, 2152.
(21) Brixner, T.; Strehle, M.; Gerber, G. *Appl. Phys. B.* **1999**, *68*, 281.
(22) Kane, D. *IEEE J. Quantum Electron*. **1999**, *35*, 421.
(23) Peatross, J.; Rundquist, A. *J. Opt. Soc. Am. B.* **1998**, *15*, 216.
(24) Paye, J. *IEEE J. Quantum Electron*. **1994**, *30*, 2693.
(25) Kapetanakos, C.; Hafizi, B.; Milchberg, H.; Sprangle, P.; Hubbard, R.; Ting, A. *IEEE J. Quantum Electron*. **1999**, *35*, 565.
(26) Osvay, K.; Ross, I. *J. Opt. Soc. Am. B.* **1996**, *13*, 1431.
(27) Zhu, W.; Rabitz, H. *J. Chem. Phys*. **1999**, *111*, 472.
(28) Engl, H.; Hanke, M.; Neubauer, A. *Regularization of Inverse Problems*; Kluwer Academic Publishers: Boston, 1996.
(29) Press, W.; Teukolsky, S.; Vetterling, W.; Flannery, B. *Numerical Recipes*; Cambridge University Press: New York, 1992.
(30) Groetsch, C. *The theory of Tikhonov regularization for Fredholm Equations of the First Kind*; Pitman Advanced Publishing Program: Boston, 1984.
(31) Paramonov, G. *Chem. Phys*. **1993**, *177*, 169.
(32) Lawton, R.; Child, M. *Mol. Phys.* **1980**, *40*, 773.
(33) Rabitz, H.; Shi, S. In *Advances in Molecular Vibrations and Collision Dynamics*; Bowman, J. M., Ratner, M. A., Eds.; JAI: Greenwich, CT, 1991.
(34) Judson, R.; Rabitz, H. *Phys. Rev. Lett*. **1992**, *68*, 1500.
(35) Toth, G.; Lorincz, A.; Rabitz, H. *J. Chem. Phys*. **1994**, *101*, 3715.
(36) Phan, M.; Rabitz, H. *Chem. Phys*. **1997**, *217*, 389.
(37) Gross, P.; Neuhauser, D.; Rabitz, H. *J. Chem. Phys*. **1993**, *98*, 4557.
(38) Bardeen, C.; Yakovlev, V.; Wilson, K.; Carpenter, S.; Weber, P.; Warren, W. *Chem. Phys. Lett*. **1997**, *280*, 151.
(39) Assion, A.; Baumert, T.; Bergt, M.; Brixner, T.; Kiefer, B.; Seyfried, V.; Strehle, M.; Gerber, G. *Science* **1998**, *282*, 919.
(40) Meshulach, D.; Yelin, D.; Silberberg, Y. *J. Opt. Soc. Am. B.* **1998**, *15*, 1615.
(41) Weinacht, T.; Ahn, J.; Bucksbaum, P. *Nature* **1999**, *397*, 233.